

SAM3D: Zero-Shot Semi-Automatic Segmentation in 3D Medical Images with the Segment Anything Model

Trevor J. Chan*, Aarush Sahni*, Jie Li*, Alisha Luthra*, Amy Fang*, Alison Pouch, and Chamith S. Rajapakse

Department of Bioengineering, Department of Radiology, University of Pennsylvania, Philadelphia, USA

Abstract. We introduce SAM3D, a new approach to semi-automatic zero-shot segmentation of 3D images building on the existing Segment Anything Model. We achieve fast and accurate segmentations in 3D images with a four-step strategy comprising: volume slicing along non-orthogonal axes, efficient prompting in 3D, slice-wise inference using the pretrained SAM, and reposition and refinement in 3D. We evaluated SAM3D performance qualitatively on an array of imaging modalities and anatomical structures and quantify performance for specific organs in body CT and tumors in brain MRI. By enabling users to create 3D segmentations of unseen data quickly and with dramatically reduced manual input, these methods have the potential to aid surgical planning and education, diagnostic imaging, and scientific research.

Keywords: Zero-shot segmentation · 3D segmentation · Semi-automatic segmentation

1 Introduction

Image segmentation is a foundational problem in both medical practice and research. Segmentation plays a critical role in surgical planning and interventional radiology [26,5], it is used to calculate common clinical metrics [10], and it is a component of many currently used and proposed diagnostic tools [3,12].

Current automated approaches to image segmentation predominantly use deep learning models trained on vast quantities of labeled data. In medicine, these models commonly achieve high performance through hyperfixation: they train on a single anatomical region imaged using a single modality. There are numerous downsides to such an approach. Training a model first requires gathering a large amount of annotated data, which can be time consuming and expensive. And, because training datasets are imperfect, these models are also susceptible to brittleness and bias. When presented with images that deviate only slightly from those in the training set, often in ways unnoticeable by humans, the models can fail unexpectedly [23,17]. Lastly, many medical imaging modalities acquire

* These authors contributed equally

3D images, which drastically increases the difficulty of storing, annotating, and processing sufficiently large and diverse datasets.

Because of this, there is a growing interest in semi-automatic approaches for general image segmentation. These methods offer a compelling compromise: by accepting a small decrease in speed and convenience compared to their fully-automated counterparts, we can have both increased reliability and greater generalizability. Previous proposed approaches to semi-automatic segmentation include early thresholding and region-growing methods for 2D and 3D, which rely on intensity values to delineate structures of interest [11]. Watershed and active contour methods segment on the basis of intensity gradients [1,8,30], and atlas and multi-atlas-based segmentation combines registration with prior knowledge in the form of an idealized reference image or set of images and labels [2,16,27]. With the advent of deep learning-based segmentation and the release of off-the-shelf models and pipelines [7,28], high-quality automatic segmentation is easier than ever, but these models still require large amounts of domain-specific training data, so researchers have sought to combine the speed and performance of deep learning methods with the generalizability of previous semi-automatic algorithms [4,24].

In 2023, Kirillov et al. introduced Segment Anything [9], a promptable semi-automatic segmentation model trained on a dataset of over 1 billion masks in a wide array of 2D images. The architecture of the segment anything model (SAM) is simple: it consists of an image encoder, a prompt encoder, and a decoder, which takes the image and prompt embedding and predicts a 2D mask. Prompting, an additional user input to inform the model of which structure to segment, could be supplied one of in four formats. Three of these: points, boxes, masks, describe the location and shape of the object of interest in the image. The fourth, text, describes the semantics of the object. Due in large part to the quantity and diversity of its training data, the segment anything model (SAM) displays remarkable zero-shot segmentation performance: it is able to segment types of images unseen during training.

In this work, we extend the SAM to 3D medical images with a novel prompting, slicing, and recomposing scheme. We test our method on a wide array of 3D medical images and show that it is capable of generating high-quality masks of diverse anatomies across a range of imaging modalities. By dramatically reducing the time and effort required to obtain 3D segmentations on unseen data, these methods have the potential to accelerate both clinical and scientific workflows and improve future fully automatic segmentation tools.

2 Methods

The method we propose for 3D segmentation is conceptually simple. Noting that SAM attains high zero-shot performance, we only need to slice a 3D image volume into a set of 2D images, add appropriate prompting to these images, segment using the pretrained model, and recombine the results into a 3D mask.

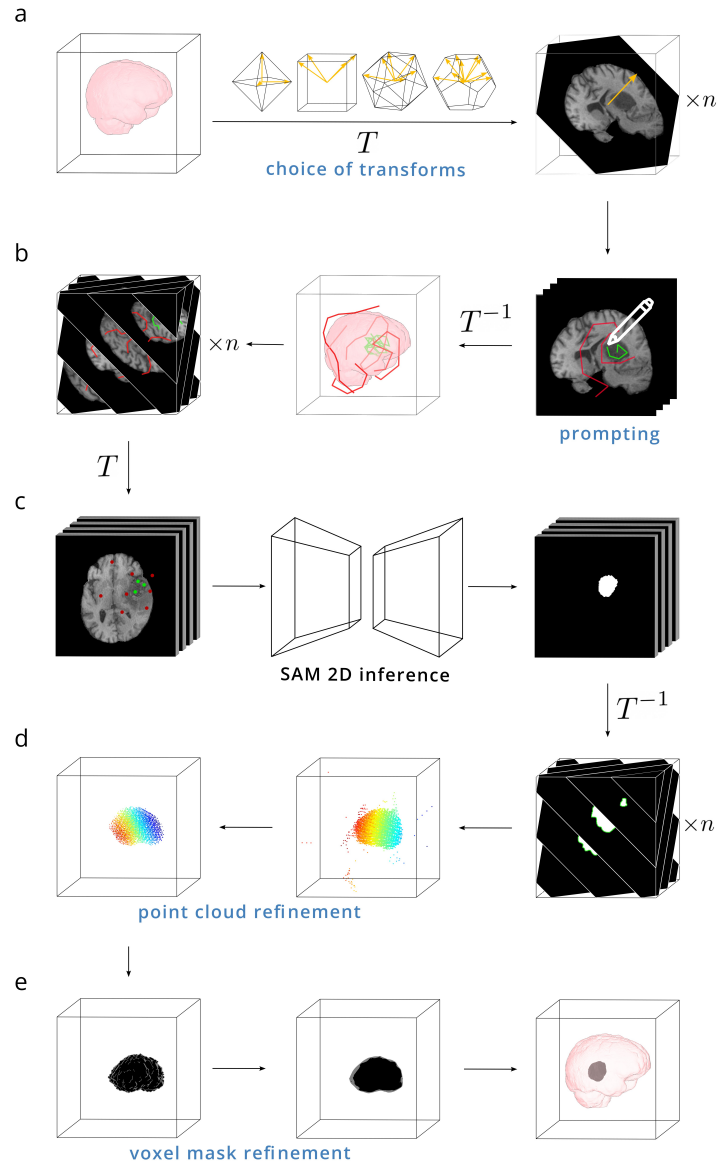


Fig. 1. An overview of the segmentation method comprising: (a) an initial choice of the number of axes to slice across (only one transform of four for cubic is shown here for clarity), (b) user prompting input as polylines to medial slices and the calculation of prompt intersection points, (c) inference on 2D slices with the pretrained SAM, (d) point extraction and user-mediated refinement of the dense point cloud, and (e) voxelization of the point cloud and user-mediated final mask refinement.

In practice, multiple decisions regarding the strategy of volume decomposition, prompting, and recomposition affect both the quality of the final 3D mask as well as the amount of human effort and time required. We select planar slices along a predefined set of n rotationally equispaced axes oriented with the vertices of a platonic solid (Figure 1a). Doing so ensures a near uniform sampling of the entire imaging region while also allowing the 2D SAM model to see each location in the imaging region n times, in essence giving it that many opportunities to segment the region correctly. Depending on the complexity of the anatomy being segmented, more or fewer axes may be called for, so the first user input is a choice of the number and distribution of axes: octahedral=3, cubic=4, icosahedral=6, and dodecahedral=10. (Once symmetries are removed, tetrahedral slicing is equivalent to cubic slicing, and is therefore omitted.)

Adding point prompts to every one of these slices, usually numbering in the hundreds, is infeasible, but it is also unnecessary. We choose only the median plane along each slicing axis to add prompting to. In contrast to SAM, which takes positive and negative prompts as 0D points, we prompt with 1D polylines that are fully contained within the structure of interest (positive) or fully outside of it (negative) (Figure 1b). We find that adding prompting to a 2D image with polylines is nearly as fast as prompting with points. But, by transforming these lines to 3D and calculating their intersections with all slicing planes along the other axes, we can generate point prompts over the entire 3D volume in an equivalent time as it would take to prompt 3-10 2D images, the number depending on the choice of transformation axes.

The resulting slices and prompt points are fed into the basic SAM model to predict a set of 2D masks suspended in 3D space (Figure 1c). As the segmentation predictions from SAM are not 100% accurate, a method for post-processing the aggregated results is needed. We convert a uniformly-sampled subset of voxels in each 2D mask to points in 3D, forming a dense 3D point cloud. While erroneous segmentation predictions in 2D result in errant points, these are extremely sparse when transformed to 3D, and can be easily and efficiently pruned with outlier detection filters (Figure 1d). The resulting dense point cloud can be voxelized and further refined using a combination of binary dilation, erosion, and hole-filling to obtain the final mask prediction (Figure 1e).

While refining the point clouds and voxel masks is both quick and intuitive, we found that the choice of parameters to use depends in part on the anatomical structure-of-interest, so each of these steps involves a small amount of user interaction to specify the aggressiveness of point cloud outlier removal and the degree of dilation and/or erosion, which affects smoothness. For a typical structure in a $256 \times 256 \times 256$ voxel image, this entire process takes on the order of minutes, roughly half of which is devoted to active user prompting and post-processing, the other half to image transformations and model inference.

To assess the accuracy and generality of our segmentation model, we tested it on a range of image modalities and anatomical structures. We selected datasets and images that capture a wide array of shapes, length scales, and image qualities (Figure 2). For image preprocessing, we resampled the image volumes into

isotropic voxel dimensions prior to input into our model. Prompting and postprocessing steps were performed by the authors, and reported times throughout the manuscript represent the duration of the full pipeline, including slicing, prompting, inference, and postprocessing. All data used is either publicly available or was approved for use in this study by an institutional review board.

We further quantified the accuracy of these segmentations using two popular 3D medical imaging datasets: one is the Beyond the Cranial Vault (BTCV) dataset for organ segmentation in abdominal CT [13], the other is the Brain Tumor Segmentation (BraTS) dataset for glioblastoma in 4 MRI contrasts [22]. Both datasets have manually labeled masks, which serve as ground truth comparisons.

3 Results

We found that the our model generated high quality masks for a range of imaging modalities and anatomical structures (Figure 2). The time required for each segmentation depended largely on the size and complexity of the anatomy being segmented; intricate structures and images with multiple components took more time to segment, but across the board our method was far faster and easier than slice-wise manual segmentation.

In the BTCV dataset, we compared segmentation performance for the liver and lungs and showed high accuracy for each (Figure 3a). In the BraTS dataset, we performed two segmentations: one for the tumor regions, comprising the enhancing tumor (ET) and necrotic/non-enhancing tumor (NCT/NET), and a second for the tumor region and the surrounding edema (ET+NCT/NET+ED). We found similarly high performance across 4 contrasts (T1, T1-contrast enhanced, T2, FLAIR) (Figure 3b). We also showed consistent mask predictions from the model for scans of the same patient with different MRI contrasts, demonstrating a robustness to pixel-level changes (Figure 3c).

To determine the effect of varying the number of transforms used for prompting and slicing, we segmented an additional 3 livers and tumors with 3, 4, 6, and 10 transforms each. We observed that for large, simple structures, such as the liver, 3 or 4 transforms, representing the octahedral and cubic axes, is sufficient. On the other hand, more complex structures, including some brain tumors, required 6+ transforms to reach peak accuracy (Figure 3d). As the amount of time and user input required for a segmentation scales with the number of transforms used, we suggest setting the number of transforms based on the complexity of the anatomy being segmented. We report the time required to segment each anatomical structure in the BTCV and BraTS dataset in table 1.

4 Discussion

We introduce a new and efficient method for prompting and inference of a pre-trained semi-automatic segmentation model and demonstrate strong results on a variety of 3D images. It is worthwhile to ask why SAM performs as well as it does



Fig. 2. Visualizing diverse segmentation performance. (a) The pelvis and sacral spine in an abdominal pelvic CT. (b) Skeleton in an *ex vivo* CT scan of the hand. (c) Cervical vertebra 3 in a CT scan of the head and neck [15]. (d) Lungs in a chest CT scan [20]. (e) Lungs, liver, and kidneys in an abdominal CT scan [13]. (f) Oxygenated blood pool in a cardiac CT scan. (g) Glioblastoma tumor and edema regions in a FLAIR MRI scan of the brain [22]. (h) Lateral ventricles, cerebellum, and brain stem in a T1 MRI scan of the brain. (i) Left ventricular outflow tract, aortic valve, and aortic root in a 3D mid-esophageal transesophageal echocardiography scan of the heart. (j) A tumor lesion in 3D breast ultrasound [25]. (k) Axonol neurons in volumetric scanning electron microscopy (SEM) of a region of the hippocampus [18]. (l) Central vacuole in volumetric SEM of a tobacco leaf cell [29].

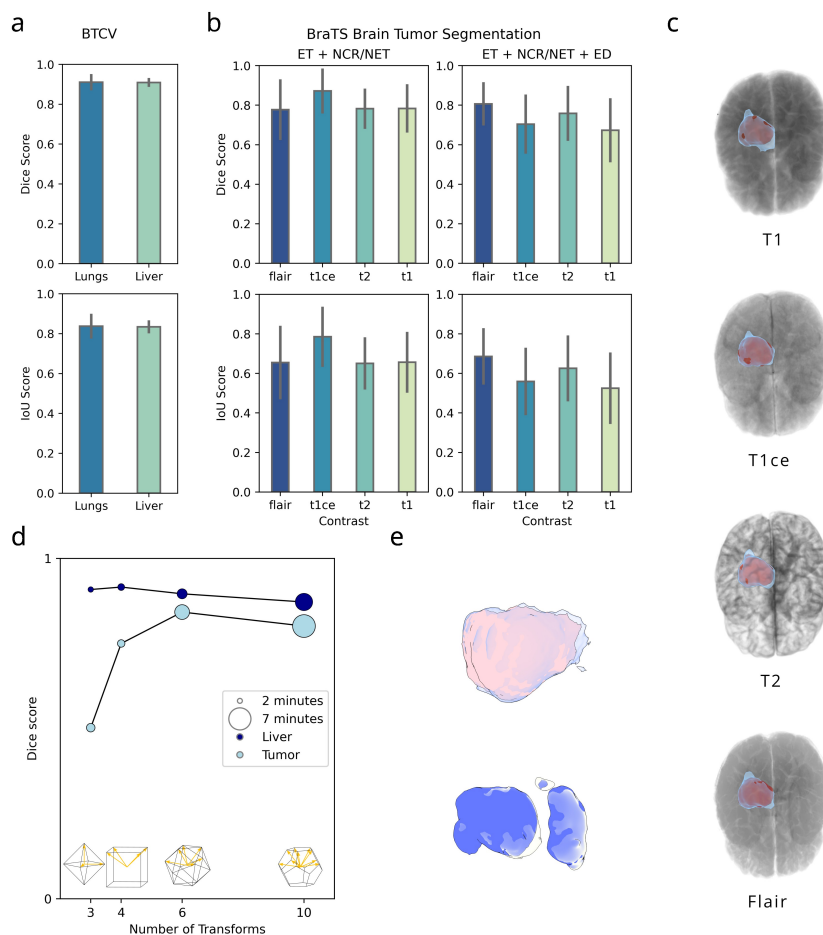


Fig. 3. Quantification of segmentation accuracy on benchmark datasets and additional experiments. (a) Dice score and intersection over union calculated for the lung and liver masks ($n = 16$) on the BTCV dataset. (b) Dice score and intersection over union calculated for the tumor region (enhanced + nonenhanced tumor/necrotic) and the tumor+edema regions ($n = 8$) for 4 MRI contrasts on the BraTS dataset. (c) Segmentation predictions for tumor and tumor+edema regions across four scans are highly consistent with each other, showing that predictions capture anatomical features and are robust to contrast, brightness, and textural changes. (d) An analysis of segmentation accuracy and time as a function of the number of transforms chosen for liver segmentation in the BTCV dataset ($n = 3$) and tumor segmentation in the BraTS dataset ($n = 3$) suggests that the optimal number of transforms to use depends heavily on the anatomical structure to segment. (e) Representative segmentation predictions (opaque) for a liver and brain tumor overlaid with the manually labeled ground-truth masks (translucent).

Table 1. A comparison of segmentation times for 5 structures across 2 common datasets.

Dataset	Segmentation Target	Time Taken (Mean +/- Std.)
BTCV[13]	Liver	4 min +/- 60 sec
	Lungs	3 min 38 sec +/- 51 sec
	Kidneys	3 min 50 sec +/- 1 min 47 sec
BraTS[22]	ET + NCT/NET	4 min 14 sec +/- 1 min 5 sec
	ET + NCT /NET+ ED	7 min 50 sec +/- 28 sec

in this task. Given that none of the images we evaluate on particularly resemble any images in the segment anything dataset, it is unreasonable to believe that the model is performing segmentations based on a semantic understanding of the data. Rather, we hypothesize that the SAM essentially mimics its much simpler precursor algorithms by relying on regional intensities, gradients, and textures to construct a hierarchical representation of the image which, when combined with prompting, can yield an accurate segmentation. While using a 2D model for 3D segmentation may seem unintuitive, this approach carries numerous benefits. It allows us to escape the memory and computational cost associated with processing 3D images. Most importantly, it allows us to leverage existing 2D datasets which, due to being easier to acquire and annotate, are far more comprehensive than their 3D counterparts.

We envision numerous uses of the proposed method. In scientific research, a method for fast semi-automatic 3D segmentation could be used in data-limited regimes or as a means to initially label training datasets. In medicine, 3D segmentation has applications in surgical planning, diagnostic imaging, and radiomics. The use of this tool could save physicians time while mitigating the risks of bias and unpredictability that plague fully automated models.

There are some notable limitations of SAM3D. As is the case for many segmentation models, including the base SAM, SAM3D has poor performance when labeling thin and branching structures. This is doubly the case in 3D, as prompt planes are sparse, so there are few opportunities to add prompting to these structures. A second limitation is that, because the base 2D segmentation model has not been trained on medical images, it lacks any relevant domain knowledge. This is potentially also an opportunity: multiple groups have taken the base SAM model and fine tuned it on a medical domain [19,6,21], and demonstrate improved results compared to the base model. Inserting these models as drop-in replacements for the SAM in our method could further improve segmentation performance and efficiency. Lastly, while we designed a rudimentary user interface for prompting and post-processing, broader use of these and similar tools would likely require a more polished interface. Other groups have shown success integrating SAM into existing medical visualization tools [14], and this is an approach we are considering.

5 Conclusion

SAM3D is a semi-automated, zero-shot 3D segmentation model capable of high performance across a range of structures and images. By enabling users to quickly, easily, and accurately segment 3D images, we hope that these methods will aid clinicians and researchers, accelerate the creation of large-scale 3D datasets, and spur development in general 3D segmentation models.

References

1. Beucher, S.: The watershed transformation applied to image segmentation. *Scanning microscopy* **1992**(6), 28 (1992)
2. Cabezas, M., Oliver, A., Lladó, X., Freixenet, J., Cuadra, M.B.: A review of atlas-based segmentation for magnetic resonance brain images. *Computer methods and programs in biomedicine* **104**(3), e158–e177 (2011)
3. Chaddad, A., Desrosiers, C., Niazi, T.: Deep radiomic analysis of mri related to alzheimer’s disease. *Ieee Access* **6**, 58213–58221 (2018)
4. Diaz-Pinto, A., Mehta, P., Alle, S., Asad, M., Brown, R., Nath, V., Ihsani, A., Antonelli, M., Palkovics, D., Pinter, C., et al.: Deepedit: deep editable learning for interactive segmentation of 3d medical images. In: *MICCAI Workshop on Data Augmentation, Labelling, and Imperfections*. pp. 11–21. Springer (2022)
5. Fang, X., Xu, S., Wood, B.J., Yan, P.: Deep learning-based liver segmentation for fusion-guided intervention. *International journal of computer assisted radiology and surgery* **15**, 963–972 (2020)
6. Huang, Y., Yang, X., Liu, L., Zhou, H., Chang, A., Zhou, X., Chen, R., Yu, J., Chen, J., Chen, C., et al.: Segment anything model for medical images? *Medical Image Analysis* **92**, 103061 (2024)
7. Isensee, F., Jaeger, P.F., Kohl, S.A., Petersen, J., Maier-Hein, K.H.: nnu-net: a self-configuring method for deep learning-based biomedical image segmentation. *Nature methods* **18**(2), 203–211 (2021)
8. Kass, M., Witkin, A., Terzopoulos, D.: Snakes: Active contour models. *International journal of computer vision* **1**(4), 321–331 (1988)
9. Kirillov, A., Mintun, E., Ravi, N., Mao, H., Rolland, C., Gustafson, L., Xiao, T., Whitehead, S., Berg, A.C., Lo, W.Y., et al.: Segment anything. *arXiv preprint arXiv:2304.02643* (2023)
10. Kitano, T., Nabeshima, Y., Otsuji, Y., Negishi, K., Takeuchi, M.: Accuracy of left ventricular volumes and ejection fraction measurements by contemporary three-dimensional echocardiography with semi-and fully automated software: systematic review and meta-analysis of 1,881 subjects. *Journal of the American Society of Echocardiography* **32**(9), 1105–1115 (2019)
11. Kohler, R.: A segmentation system based on thresholding. *Computer Graphics and Image Processing* **15**(4), 319–338 (1981)
12. Lambin, P., Leijenaar, R.T., Deist, T.M., Peerlings, J., De Jong, E.E., Van Timmeren, J., Sanduleanu, S., Larue, R.T., Even, A.J., Jochems, A., et al.: Radiomics: the bridge between medical imaging and personalized medicine. *Nature reviews Clinical oncology* **14**(12), 749–762 (2017)
13. Landman, B., Xu, Z., Iglesias, E., Styner, M., Langerak, R., Klein, A.: Multi-atlas labeling beyond the cranial vault—workshop and challenge (2015). <https://doi.org/https://doi.org/10.7303/syn3193805>

14. Liu, Y., Zhang, J., She, Z., Kheradmand, A., Armand, M.: Sann (segment any medical model): A 3d slicer integration to sam. arXiv preprint arXiv:2304.05622 (2023)
15. Löffler, M.T., Sekuboyina, A., Jacob, A., Grau, A.L., Scharf, A., El Hussein, M., Kallweit, M., Zimmer, C., Baum, T., Kirschke, J.S.: A vertebral segmentation dataset with fracture grading. *Radiology: Artificial Intelligence* **2**(4), e190138 (2020)
16. Lötjönen, J.M., Wolz, R., Koikkalainen, J.R., Thurfjell, L., Waldemar, G., Soininen, H., Rueckert, D., Initiative, A.D.N., et al.: Fast and robust multi-atlas segmentation of brain magnetic resonance images. *Neuroimage* **49**(3), 2352–2365 (2010)
17. Lu, L., Ehmke, R.C., Schwartz, L.H., Zhao, B.: Assessing agreement between radiomic features computed for multiple ct imaging settings. *PloS one* **11**(12), e0166550 (2016)
18. Lucchi, A., Smith, K., Achanta, R., Knott, G., Fua, P.: Supervoxel-based segmentation of mitochondria in em image stacks with learned shape features. *IEEE transactions on medical imaging* **31**(2), 474–486 (2011)
19. Ma, J., He, Y., Li, F., Han, L., You, C., Wang, B.: Segment anything in medical images. *Nature Communications* **15**(1), 654 (2024)
20. Ma, J., Wang, Y., An, X., Ge, C., Yu, Z., Chen, J., Zhu, Q., Dong, G., He, J., He, Z., et al.: Toward data-efficient learning: A benchmark for covid-19 ct lung and infection segmentation. *Medical physics* **48**(3), 1197–1210 (2021)
21. Mazurowski, M.A., Dong, H., Gu, H., Yang, J., Konz, N., Zhang, Y.: Segment anything model for medical image analysis: an experimental study. *Medical Image Analysis* **89**, 102918 (2023)
22. Menze, B.H., Jakab, A., Bauer, S., Kalpathy-Cramer, J., Farahani, K., Kirby, J., Burren, Y., Porz, N., Slotboom, J., Wiest, R., et al.: The multimodal brain tumor image segmentation benchmark (brats). *IEEE transactions on medical imaging* **34**(10), 1993–2024 (2014)
23. O’connor, J.P., Aboagye, E.O., Adams, J.E., Aerts, H.J., Barrington, S.F., Beer, A.J., Boellaard, R., Bohndiek, S.E., Brady, M., Brown, G., et al.: Imaging biomarker roadmap for cancer studies. *Nature reviews Clinical oncology* **14**(3), 169–186 (2017)
24. Roy, A.G., Siddiqui, S., Pölsterl, S., Navab, N., Wachinger, C.: ‘squeeze & excite’guided few-shot segmentation of volumetric images. *Medical image analysis* **59**, 101587 (2020)
25. Tumor detection, segmentation and classification challenge on automated 3d breast ultrasound (abus) 2023 (2023)
26. Virzì, A., Müller, C.O., Marret, J.B., Mille, E., Berteloot, L., Grévent, D., Boddart, N., Gori, P., Sarnacki, S., Bloch, I.: Comprehensive review of 3d segmentation software tools for mri usable for pelvic surgery planning. *Journal of digital imaging* **33**(1), 99–110 (2020)
27. Wang, H., Pouch, A., Takabe, M., Jackson, B., Gorman, J., Gorman, R., Yushkevich, P.A.: Multi-atlas segmentation with robust label transfer and label fusion. In: *Information Processing in Medical Imaging: 23rd International Conference, IPMI 2013, Asilomar, CA, USA, June 28–July 3, 2013. Proceedings* 23. pp. 548–559. Springer (2013)
28. Wasserthal, J., Breit, H.C., Meyer, M.T., Pradella, M., Hinck, D., Sauter, A.W., Heye, T., Boll, D.T., Cyriac, J., Yang, S., et al.: Totalsegmentator: Robust segmentation of 104 anatomic structures in ct images. *Radiology: Artificial Intelligence* **5**(5) (2023)

29. Wickramanayake, J.S., Czymmek, K.J.: A conventional fixation volume electron microscopy protocol for plants. *Methods in Cell Biology* **177**, 83–99 (2023)
30. Yushkevich, P.A., Piven, J., Hazlett, H.C., Smith, R.G., Ho, S., Gee, J.C., Gerig, G.: User-guided 3d active contour segmentation of anatomical structures: significantly improved efficiency and reliability. *Neuroimage* **31**(3), 1116–1128 (2006)